corrosion and materials degradation

MDPI

Article

Development of Photocatalytically Active Anodized Layers by a Modified Phosphoric Acid Anodizing Process for Air Purification

Stephan Lederer [1,*], Sigrid Benfer [1], Jonathan Bloh [1], Rezan Javed [1,2], Aneta Pashkova [1] and Wolfram Fuerbeth [1]

[1] DECHEMA Research Institute, 60486 Frankfurt am Main, Germany
[2] Advanced Functional Materials, Chemnitz University of Technology, 09111 Chemnitz, Germany
* Correspondence: stephan.lederer@dechema.de

Abstract: One of the key urban air quality issues is pollution by nitrogen oxides (NO_x). To reduce NO_x, facade cladding could be provided with photocatalytic properties by incorporating titanium dioxide nanoparticles. For this purpose, a modified phosphoric acid anodizing process (MPAA) was developed for the facade alloy EN AW-5005, in which highly ordered anodized structures with a low degree of arborization and tortuosity were produced. Pore widths between 70 nm and 150 nm and layer thicknesses of about 2–3 µm were obtained. The subsequent impregnation was carried out by dip coating from water-based systems. Depending on the dip-coating parameters and the suspension used, the pores can be filled up to 60% with the TiO_2 nanoparticles. Photocatalytic tests according to ISO 22197-1 certify a high photocatalytic activity was obtained with rPCE values > 8 and with rPCE > 2, achieving "photocatalytically active for air purification". Tests on the corrosion resistance of the anodized coatings with a commercially available aluminum and facade cleaner confirm a protective effect of the anodized coatings when compared with nonanodized aluminum material, as well as with compacted anodized layers.

Keywords: aluminum; anodizing; photocatalysis; titanium dioxide; nitrogen oxide; dip coating; nanoparticle

Citation: Lederer, S.; Benfer, S.; Bloh, J.Z., Javed, R.; Pashkova, A.; Fuerbeth, W. Development of Photocatalytically Active Anodized Layers by a Modified Phosphoric Acid Anodizing Process for Air Purification. *Corros. Mater. Degrad.* **2023**, *4*, 18–30. https://doi.org/10.3390/cmd4010002

Academic Editor: Henryk Bala

Received: 21 November 2022
Revised: 15 December 2022
Accepted: 21 December 2022
Published: 31 December 2022

1. Introduction

The emission of nitrogen oxides (NO_x) is currently one of the main problems for air quality in urban areas. The German Federal Environment Agency (UBA) evaluating annual NO_x mean values found that, in 2019, around 12% of the measuring stations in Germany exceeded the European limit of nitrogen dioxide (NO_2) [1]. Compared with the WHO recommendation to reduce the current limits from 40 μgm^{-3} to 10 μgm^{-3}, 88% of all measuring stations exceeded this level [2]. Around 60% of all NO_x emissions are related to mobility and housing.

To reduce the concentration of nitrogen oxides, photocatalytic reactions can be initiated under the influence of light, thus converting harmful NO_x into nitrate (NO_3^-). The nitrate formed on the surface is easily soluble in water and is absorbed and transported away by condensation, rain, or cleaning water. This property is currently in use in some building materials, such as photocatalytically active roof surfaces, facade paints, coated paving stones or tunnel linings [3–6].

Aluminum is considered an important material in the construction industry and is often used—in anodized form—for large-scale cladding of facades and roofs. Each aluminum facade with a photocatalytic coating could thus contribute to a reduction in the concentration of nitrogen oxides in the atmosphere. In contrast to mild steels, aluminum generally shows good corrosion resistance. Aluminum forms a native oxide layer, with a thickness of up to 15 nm [7]. Since the protective properties of the native passive layer can be limited, the thickness is increased using the "electrolytic oxidation of aluminum (ElOxAl)" process.

The layer is usually produced in an anodizing process using sulfuric acid, oxalic acid or phosphoric acid [8–13]. In general, the layer properties can be controlled via the type of the electrolyte and the concentration and variation of the process parameters (voltage, time, bath circulation and bath temperature) [14]; electrolyte, voltage and bath temperature are considered to have the greatest influence in the anodizing process [13,15–17]. Subsequently, the resulting mesoporous oxide layer is typically sealed or dyed using metal salts of tin, nickel or (in)organic dyes [18–20].

Recent progress in the development of colloidal systems makes it possible to use the open-pore structure of anodized aluminum to generate new functional properties. The principle is similar to the dyeing of the layers and is based on the incorporation of nanoparticles into the pores of the anodized layer [21,22]. Phosphoric acid anodizing (PAA) enables the formation of large open-pore structures with pore widths up to ∼150 nm, which is not possible for the more common sulfuric acid anodizing (SAA) [13,23]. Within this context, the commercial availability of photocatalytically active TiO_2 nanoparticles ($\varnothing$ < 20 nm) is also essential [24,25]. When a photocatalyst is exposed to sunlight, reactive charge carrier pairs (electrons and holes) are formed, which react with oxygen or water molecules in a first reaction step, generating highly reactive superoxide (O_2^- •) or hydroxyl (OH•) radicals, which further oxidize pollutant molecules [26,27]. To classify the photocatalytic activity, products are tested according to ISO 22197-1, and the relative photocatalytic efficiency (rPCE) is determined. If rPCE > 2 is achieved, the reduction in NO_x is sufficient, and the product is beneficial to be used for air purification.

The aim of this work was to generate open-porous-structured anodized layers feasible for the subsequent incorporation of photocatalytically active titania nanoparticles via dip coating. The chosen anodizing conditions were based on the literature [28,29] and are further developed using a factorial Design of Experiments (DoE) to optimize the resulting layer with respect to the coating thickness and pore size. Subsequently, the functionalized layers were examined regarding their photocatalytic activity and corrosion resistance.

2. Materials and Methods

The procedure to generate a photocatalytically active anodized layer consists of two steps: (1) the formation of open porous anodized layers, and (2) the incorporation of commercially available titania nanoparticles into the pores of the anodized layer. The pore structure of the anodized layer is intended to act as a "vessel" for the titanium dioxide nanoparticles incorporated via dip coating to retain the photocatalytic properties, even if an abrasive facade cleaning process is applied. The decisive factor is the use of small photoactive TiO_2 nanoparticles (ideally: particle size $\leq$ 20 nm). Additionally, the barrier properties of the anodized layer are expected to be improved in terms of aqueous corrosion protection by filling the pores with nanocrystalline titanium dioxide.

2.1. Phosphoric Acid Anodization

Since titania nanoparticles will be embedded into the anodized layers, open pores with diameters of around 100 nm are required. In addition to the voltage and other parameters, the cell/pore size to be achieved depends strongly on the acid used, in this case, phosphoric acid.

Sheets of the aluminum alloy AlMg1 (EN AW-5005) were used as the substrate. Before anodizing, the substrate was degreased in an alkaline etchant (Bonderite C-AK 62018) at 60 °C for 10 min, etched in a caustic soda solution (Bonderite C-AK 62251, 50 °C, 5 min) and pickled in nitric acid at room temperature for 2 min. After the pretreatment procedure, the anodization was carried out using direct current. A Cr/Ni steel sheet was used as the cathode and connected to the aluminum sheet as the anode. The surface area of the cathode was 150 cm^2 and the surface area of the aluminum sample was 3 cm^2. The electrodes were connected above the bath level.

A modified phosphoric acid anodization (MPAA) process was developed, and the influence of the process parameters, in particular bath temperature, voltage and treatment

time, were examined with respect to the optimized target parameters such as pore size and layer thickness. Using a 2^3 full factorial design of experiments and the following parameter set, the resulting layers were characterized in terms of the following properties (Table 1):

Table 1. Design of Experiments.

Factor	Range	Response	Target
Bath temperature	35–45 °C	Pore size	>100 nm
Voltage	40–55 V	Layer thickness	2–4 µm
Anodizing time	60–420 s	Layer quality	Homogeneous, open pores
Phosphoric acid concentration	10–20 wt.%		

The influence of the different anodizing conditions on the resulting anodized layers and pore structure is described and discussed in detail in Chapter 3.1.

2.2. Dip Coating

For the incorporation of the titania nanoparticles, two commercial dispersions were used, Evonik Aerodisp W2730X (30% TiO_2) diluted to a solid content of 15% and a dispersion from Tronox (CristalACTiV PC-S7, solid content 10%). According to the manufacturer's information in all dispersions, the titanium dioxide was present in the anatase modification. For the W2730X dispersion, the primary particle size was specified as 14 nm. For the PC-S7 dispersion, the specific surface area of the particles was given as 300 m^2g^{-1}. The particle size of the TiO_2 nanoparticles present in the dispersions was also measured using dynamic light scattering *DLS* (ZetasizerNano ZS, Malvern Panalytical). This method gives the hydrodynamic diameter of the particles. The measured mean particle size of the number distribution was about 70 nm for the W2730X dispersion. The mean particle size in the dispersion PC-S7 is significantly lower at approximately 38 nm. In all dispersions, the values were larger compared with the primary particle size of the titanium dioxide powders, suggesting an agglomeration of the particles in the dispersions.

A computer-controlled dip coater (KSV Instruments) was used to carry out the dip coating experiments to obtain reproducible results. According to the Landau–Levich equation, the solid content of the dispersion (i.e., influence on viscosity and density) and the withdrawal speed are the main parameters influencing the wet film thickness, and thus the number of particles available for incorporation [30]. To break up possible particle agglomerates, the dispersions were treated in an ultrasonic bath for 10 min before dip coating. All samples were impregnated "wet-in-wet" to prevent possible repelling. Following dip coating experiments were carried out:

1. PC-S7 (10 wt.% TiO_2, pH 8, particle size (DLS) ~38 nm)
   - withdrawal speed: 40 mm/min, 50 mm/min.
2. W2730X (15 wt.% TiO_2, pH 7, particle size (DLS) ~70 nm)
   - withdrawal speed: 10 mm/min.

After dip coating, the samples were fractured and investigated by scanning electron microscopy (SEM) and energy-dispersive X-ray spectroscopy (EDS) with respect to the amount of incorporated nanoparticles.

2.3. Photocatalytic Activity

The photocatalytic activity of the anodized layers incorporated with TiO_2 particles was determined in a photoreactor measuring the NO degradation according to ISO 22197-1. The total gas flow during the measurement was 3 L/min at a relative humidity of 50% and an NO concentration of 1 ppm in synthetic air. The UV irradiation in the reactor had a power of 1 $mWcm^{-2}$. The total irradiated area was 50 cm^2, and the test duration was fixed to 5 h.

Initially, the absolute amount of eliminated NO over 5 h was determined and compared with the maximum degradable amount of test gas which passed the reactor within the

irradiation period. From this, the rPCE value was calculated. The rPCE value indicates the relative photocatalytic efficiency. Products for photocatalytic air purification achieving rPCE > 2 can be designated as "photocatalytically active for air purification according to the FAP self-commitment" [31].

2.4. Corrosion Investigations

Depending on the application, different cleaners are used to clean anodized surfaces. For this reason, the corrosion resistance of the functionalized surface was tested with a commercially available aluminum and facade cleaning solution (Clever-AS-Technik GmbH), dilution 1:20 and pH 1.8. A standard 3-electrode setup in an Avesta cell with vertical sample installation, an Ag/AgCl reference electrode and a platinum counter electrode (2×2 cm^2) were used for the corrosion investigations. The measurement sequence started with a 60 min measurement of the open-circuit potential, followed by a measurement of the electrochemical impedance in the range from 10 mHz to 100 kHz, with an amplitude of 10 mV and a final potentiodynamic polarization from −50 mV to +400 mV vs. OCP with a scan rate of 0.5 mVs^{-1}. The following samples were tested:

- Aluminum sheet EN-AW5005 pretreated (degreased, etched and pickled).
- MPAA sample.
- MPAA sample incorporating TiO_2 particles (Tronox PC-S7).
- Oxalic acid anodized sample, sealed (benchmark; c = 57 g/L, V = 46 V, T = 20 °C; d_{pore} = 40–60 nm, d_{layer} ~2 µm).

3. Results and Discussion

3.1. Phosphoric Acid Anodizing

In Figure 1, the surface structure and thickness of layers anodized for 60 s and 420 s at a voltage of 55 V and a temperature of 35 °C is shown. For longer anodizing times (420 s), pore sizes of >100 nm and layer thicknesses of approximately 3.5 µm are achieved. However, it is also evident that the deposits formed on the surface after long anodizing times might hinder the incorporation of titania particles. Therefore, the interaction of the process parameters was studied in more detail to optimize the resulting layers.

Evaluation of the DoE shows that temperature and voltage have the greatest influence on the pore width, while the anodizing time has less influence at a certain given voltage. Figure 2 shows the dependence of the pore size as a function of temperature, time, and voltage displayed in a response surface plot. At very high voltages (55 V to 60 V) at 45 °C, a pore size of >150 nm could be generated. However, the anodizing process is not stable under these conditions, since small crevices or edges lead to an uncontrolled current increase. According to the DoE response, the target pore size of 100 nm is also achieved under the more moderate conditions of T = 41–43 °C and V = 50–55 V (at an anodizing time of 180 s).

At a given temperature and voltage, longer anodizing times lead, compared with the interaction of temperature and voltage, to only a relatively small increase in the pore size (Figure 2b). However, only in the beginning, there is a linear relationship between the pore size/coating thickness and the anodizing time, but for longer dwell times after a steep increase in the initial process, an establishment of a rather stable plateau can be observed, indicating the equilibrium between the formation of the anodizing layer and a re-dissolution process (Figure 3a).

According to previous studies [32,33], the formation and solution of alumina occurs simultaneously, i.e., there is a dynamic balance during the anodizing treatment. On one hand, the dissolution taking place at the cell walls leads to an increase in the pore diameter with the anodizing time (comparing Figure 1); on the other hand, the rate of oxide formation is a function of electric current and time according to Faraday's law. At the point when this proportionality is no longer given, the dissolution-related limit is reached [28]. As a comparison, in Table 2, the total accumulated amount of charge versus the measured

coating thickness for selected treatment conditions is given. It is obvious that for increasing temperatures a linear relationship no longer exists.

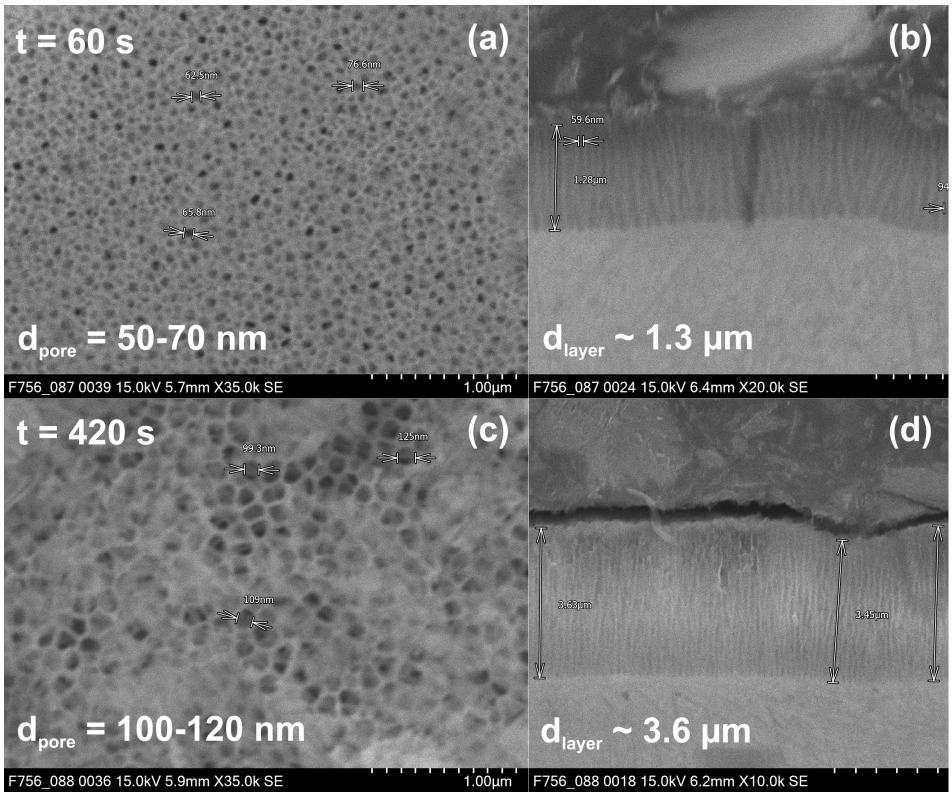

Figure 1. Influence of anodizing time on pore size and layer thickness (bath temperature 35 °C and Voltage 55 V). (**a**,**b**) t = 60 s; (**c**,**d**) t = 420 s .

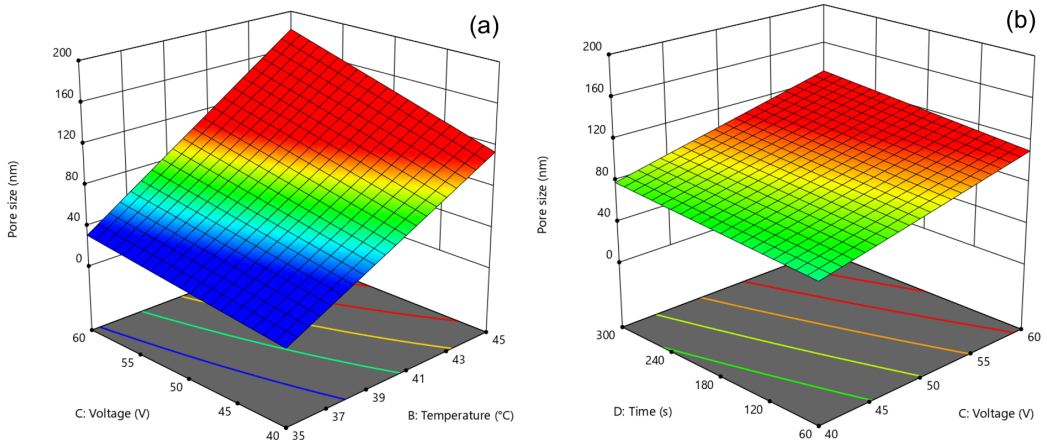

Figure 2. Three-dimensional surface plots evaluating the influence of DoE factors on the pore size. (**a**) temperature and voltage; (**b**) time and voltage.

Due to the increased re-dissolution rate at higher temperatures, the layer thickness remains constant at shorter times, while it is even reduced for longer treatments (Figure 3b). Consequently, the layer thickness anodized at 45 °C (40 V and 420 s) is lower than the layer thickness obtained at 35 °C (under otherwise identical conditions).

Overall, the results show that pore sizes of around 100 nm, as desired for impregnation, as well as sufficiently high layer thicknesses are achieved at voltages of >45 V. However, the surface quality must also be considered. As mentioned previously for longer anodizing times, the formation of a so-called "bird's nest" structure is observed, which prevents open access to the pores and should therefore be avoided. The appearance of this whisker-like

structures is attributed to the formation and collapse of thinned oxidic filaments. This phenomenon is well-known and is related to the process conditions such as acid type, concentration, temperature and dwell time [28,34]. Initially, 20 wt.-% phosphoric acid was used, where this effect occurs already after an anodizing time of 180 s (Figure 4). For this reason, the acid concentration was reduced to 10 wt.-%. As a result, the bird nest structures appear after anodizing times of approximately 300 s, which means that a reduction in the acid concentration has a clear positive influence on the surface quality. At the same time, the pore size is only slightly reduced.

Table 2. Obtained coating thickness for different temperatures and dwell times at a constant voltage of V = 40 V.

Temperature °C	Dwell time s	Charge accumulated Ccm^{-2}	Coating thickness µm
35	60	1.79	1.0 ± 0.1
35	420	5.87	2.2 ± 0.2
45	60	6.65	1.9 ± 0.1
45	420	23.21	2.1 ± 0.1

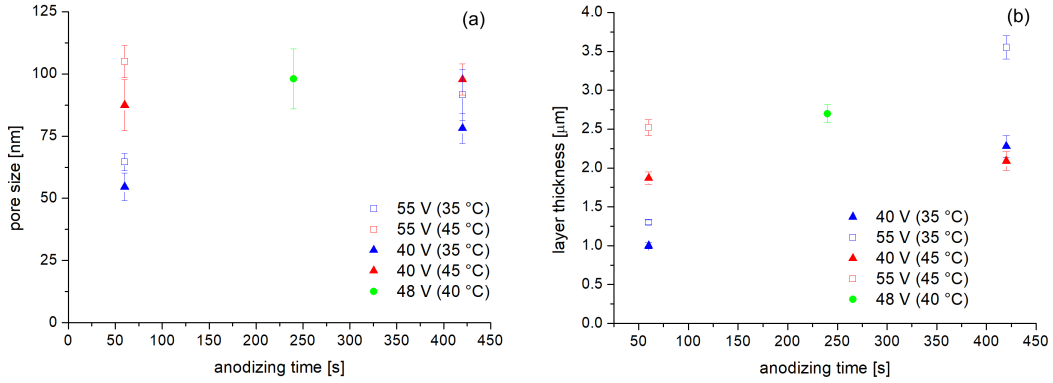

Figure 3. (**a**) Pore size and (**b**) layer thickness as a function of anodizing time at different voltages and temperatures.

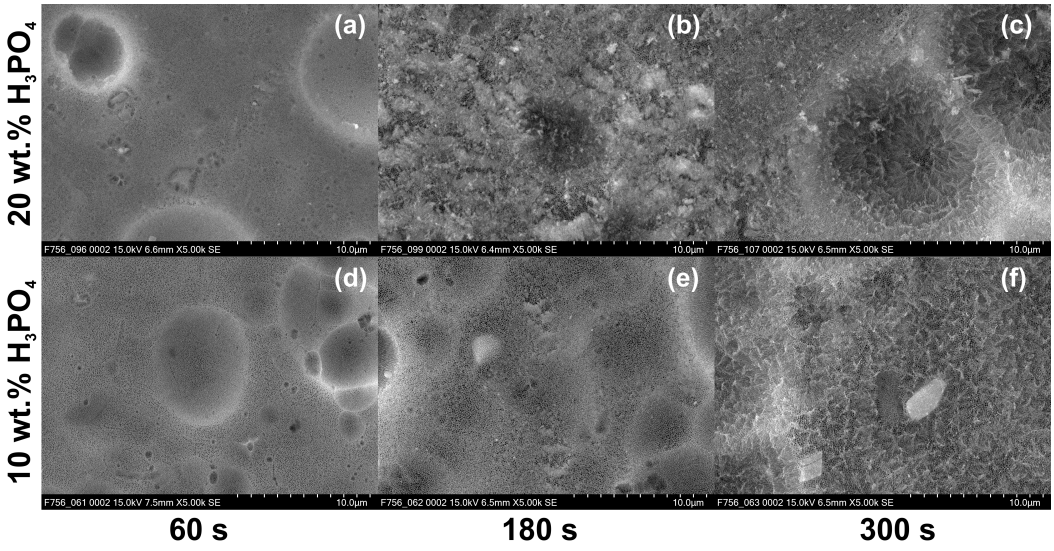

Figure 4. SEM micrographs of anodized surfaces obtained at different acid concentrations. (**a**,**b**,**c**) 10 wt.-%; (**d**,**e**,**f**) 20 wt.-% (bath temperature 40 °C, voltage 50 V).

Finally, the following set of parameters was determined to be the optimum with regards to forming the correct pore size and surface quality (an open-pore structure which avoids bird nest formation):

- Electrolyte: 10 wt.-% phosphoric acid.
- Temperature: 42 °C .
- Voltage: 55 V.
- Anodizing time: 180 s.

As Figure 5 shows, with these parameters, an anodized layer with a thickness of approximately 2 µm and an open-pore structure with pore widths of 85–105 nm is produced.

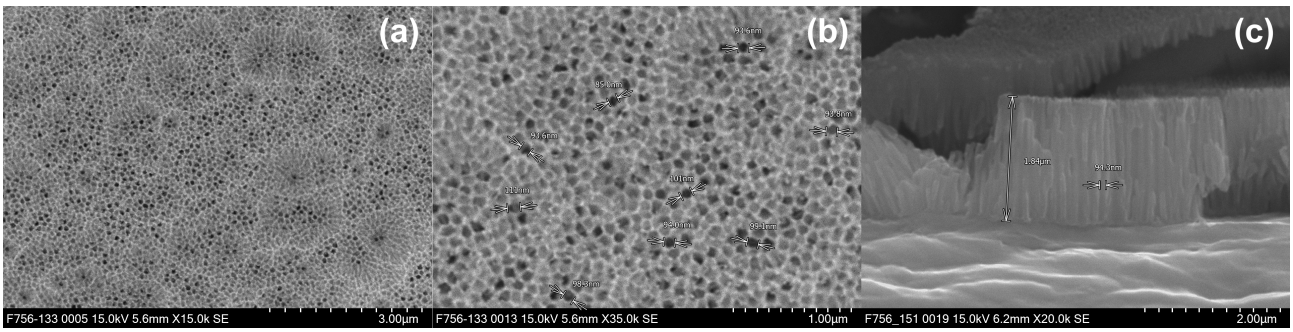

Figure 5. (**a**–**c**) SEM micrograph of surface and fractured cross-section of the optimized anodized layer.

3.2. Dip Coating

The dip-coating parameters were adjusted to increase the degree of filling in the pores, i.e., the photocatalytic activity of the layers. For this purpose, drawing speeds of up to 50 mm/min and solid contents of up to 30 wt.% were tested. Despite the high solids content of the dispersions, the optical appearance of the anodized layers is hardly affected by the impregnation. Compared with the nonimpregnated sample, the anodized and impregnated surface appears to be slightly more opaque. If the dispersion W2730X is used with an initial solid content of 30 wt.%, a continuous, two-dimensional topcoat is formed despite the low withdrawal speed of 10 mm/min. SEM micrographs of the fractured surfaces of the impregnated sample (not shown here) reveal that not only a layer of several hundred nanometers thickness is formed on the surface, but some individual particles are also incorporated into the pores of the anodized layer. Measurements of the particle size give 14 nm to 20 nm in diameter, which is significantly lower than the hydrodynamic diameter measured with DLS. However, the value corresponds to the primary particle size specified by the manufacturer for the TiO_2 particles used. The primary particle size would therefore allow incorporation into the 100 nm pores of the anodic layers. However, the additives used to stabilize the high solid dispersion cause the layer to form preferentially on the surface. Since this formed top layer can be easily wiped away, and would thus be a waste of material, the solid content of the Evonik dispersion was reduced to 15 wt.%.

In Figure 6, SEM micrographs of fractured samples of the anodized layers impregnated with PC-S7 (a) and W2730X (b) dispersions are shown. With the PC-S7 dispersion, a pore filling of approx. 30–50 wt.% is achieved. The TiO_2 particles adhere to the pore walls, indicating attractive interactions between the negatively charged particles and positively charged pore walls. A reduction in the solid content to 15 wt.% for the Evonik W2730X dispersion also reduces the layer formed on the surface of the impregnated anodized layers. However, only a few particles entered the pores, since the particle size increased significantly to 25–45 nm when compared with the undiluted dispersion (14–20 nm).

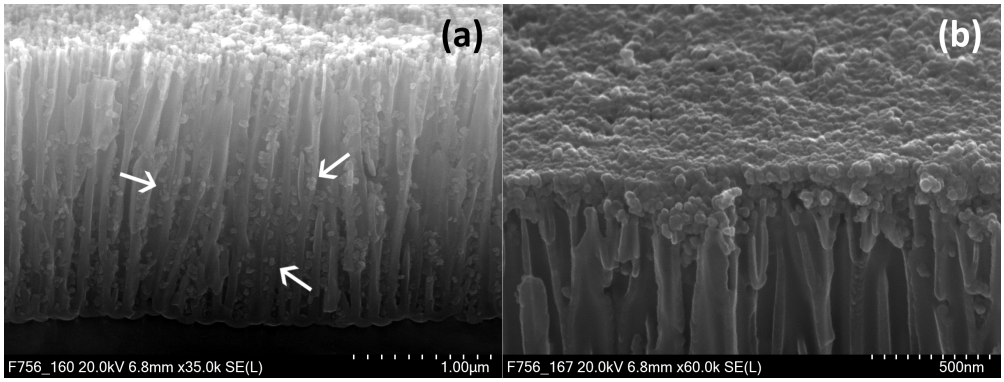

Figure 6. Fractured cross-sections of anodized layers impregnated with Tronox PC-S7 (**a**) and Evonik W2730X (**b**). Titania particles are marked exemplarily by arrows.

3.3. Photocatalytic Activity

In Figure 7, the NO concentration as a function of time upon UV irradiation of the anodized layers impregnated with Tronox PC-S7 (40 mm/min) (a) and Evonik W2730X (15 wt.%, 10 mm/min) (b) is displayed. All samples show a clear photocatalytic activity as indicated by a lowered NO concentration under UV light. For the sample impregnated with the W2730X dispersion, a significantly higher photocatalytic activity is obtained compared with the PC-S7 sample.

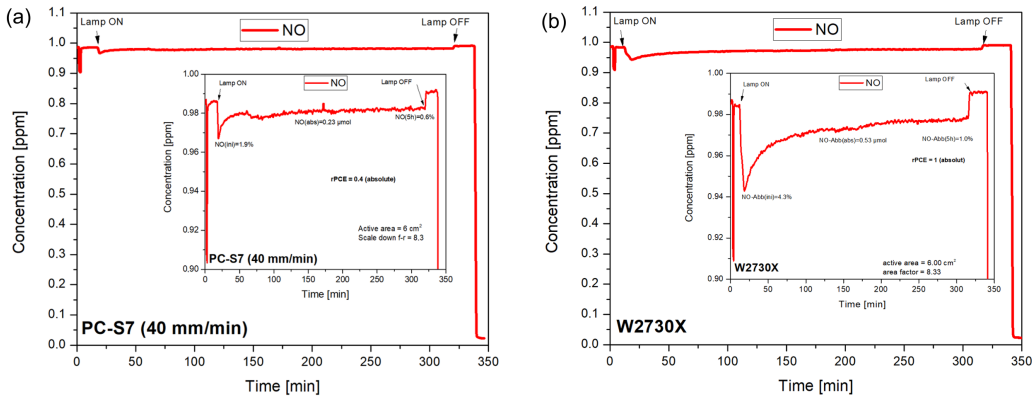

Figure 7. Time-dependent NO concentration of the anodized layers impregnated with PC-S7 (40 mm/min) (**a**) and W2730X (15 wt.%, 10 mm/min) (**b**).

This observation can be explained by the different degree of surface coverage. For the sample impregnated with the PC-S7 dispersion, the titania particles are present mainly inside the pores and deposits can be found only in the etching dimples (Figure 8, right), while the samples impregnated with W2730X show a significantly thicker and more extensive coating. To investigate the influence of the surface depositions, and in order to reduce them if possible, the samples were wiped off with a lint-free paper towel several times. Then, a second measurement of the photocatalytic activity was performed. Interestingly, the sample impregnated with PC-S7 (40 mm/min) showed even a slight increase in the photocatalytic activity after this treatment (Figure 8, left).

SEM micrographs of wiped surfaces show (Figure 8, right) that the titania-rich deposits are still present, and the particles adhere very well to the surface. Overall, all tested samples show an rPCE value > 2 and are therefore considered to be photocatalytically active for air purification. (Table 3).

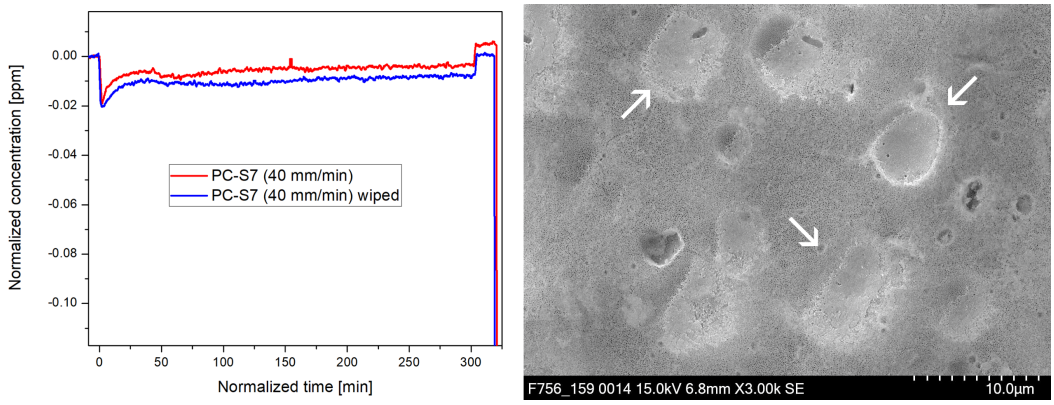

Figure 8. Comparison of NO reduction in the anodized layer impregnated with PC-S7 (40 mm/min) before and after wiping (**left**) and SEM micrograph of the surface impregnated with PC-S7 dispersion and wiped with a cloth (**right**). Residual titania deposits are still present in etching dimples and marked by arrows.

Table 3. NO degradation rate and rPCE values of the impregnated anodizing layers.

Sample Code	NO Degradation Abs. [µmol]	rPCE
PC-S7-1	1.9	3.6
PC-S7-2	3.4	6.3
PC-S7-3	4.4	8.4
PC-S7-4	2.7	5.0
W2730X-1	4.4	8.4
W2730X-2	4.5	8.4

3.4. Corrosion

Since the functionalized anodized layers are to be applied as facade claddings, their corrosion resistance was tested with respect to a commercially available aluminum and facade cleaner. In a typical dilution of 1:20, as specified by the manufacturer, the cleaner has a pH-value of 1.8. In Figure 9, the open-circuit potentials (OCP) of pristine AlMg1, MPAA anodized and impregnated samples, as well as an oxalic acid anodized sample, are shown. The OCP of the pristine, i.e., only pretreated, AlMg1 sample shifts from an initial potential of approx. −0.27 V vs. SHE to −0.4 V vs. SHE within 60 min. The anodized and partially compacted or impregnated surfaces show very different values at the beginning of the measurement, but all stabilize at a similar value of around −0.1 V vs. SHE. Overall, all anodized layers exhibit an OCP that is approx. 300 mV more positive than the pristine AlMg1 surface, whereas the OCP of the compacted oxalic acid anodized layer is slightly more positive (−0.05 V vs. SHE) than the MPAA samples.

The protective effect of the anodized surfaces is confirmed by electrochemical impedance spectroscopy (Figure 10). The impedance modulus at low frequencies can be considered as the sum of all system resistances. Since the solution resistance is negligible in this case, it can be used as a first approximation for the polarization resistance R_p. In the low-frequency range, the reference sample anodized in oxalic acid reaches impedance values > 1 MΩcm^2, which are at least two orders of magnitude higher than the pristine surfaces (∼10 kΩcm^2). The compaction of the layer leads to a further increase in the impedance values when compared with noncompacted layers. The impregnated MPAA samples exhibit an even more protective effect than the layer produced in oxalic acid, reaching impedance values > 10 MΩcm^2 at low frequencies. The impedance values increase almost uniformly over the entire frequency range, indicating a capacitive behavior and an excellent barrier effect of the layers. The introduction of the TiO_2 particles into the layer leads to further increases in the barrier effect (Figure 10). The high impedance values of the MPAA samples when compared with the oxalic acid anodized samples can be explained

by the formation of a denser barrier layer, since the pores formed in phosphoric acid are larger in size but less in number [35]. Moreover, the barrier characteristics depend as well upon the process conditions, i.e., in particular the pore resistance increases with increasing temperature [35] and the barrier layer thickness increases with increasing voltages [28,36].

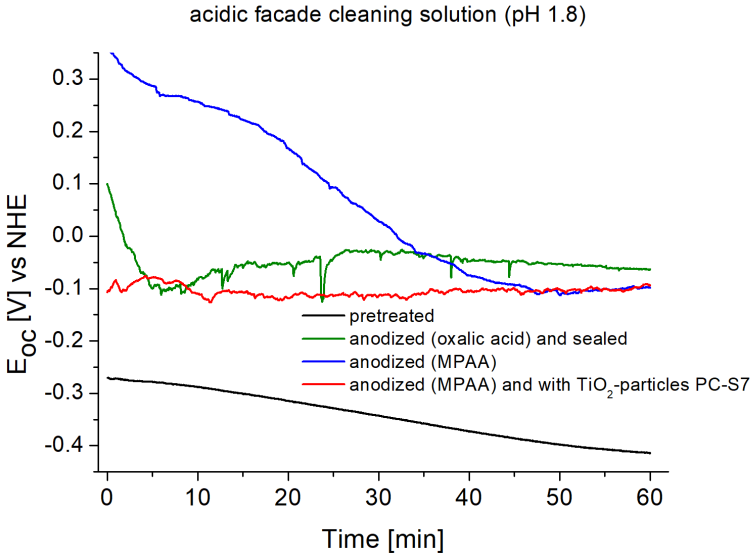

Figure 9. Development of open-circuit potential for different AlMg1 samples.

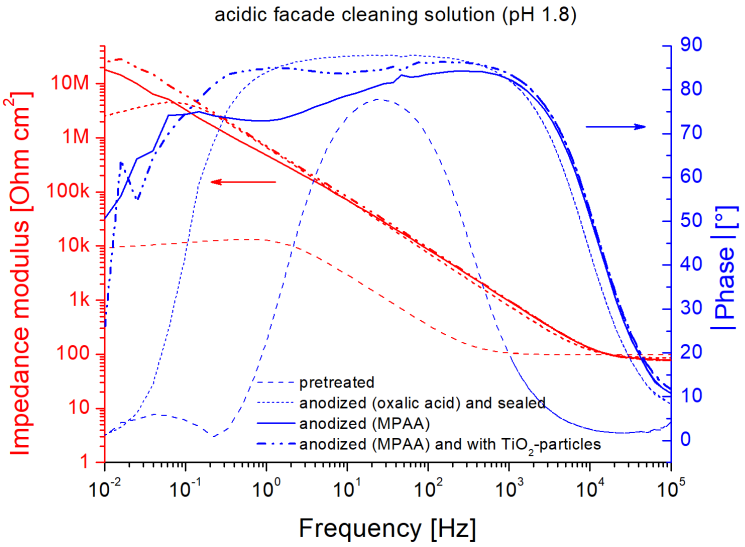

Figure 10. Bode plot of impedance spectra of AlMg1 treated under different conditions.

Additional potentiodynamic polarization measurements in the same acidic facade cleaning solution again demonstrate the good corrosion protection provided by anodized layers (Figure 11). The pristine AlMg1 material exhibits corrosion current densities of 1.5–2 μAcm^{-2}. In comparison, for the MPAA samples, the corrosion current densities are in the range from 10^{-9} Acm^{-2} to 10^{-12} Acm^{-2}. Overall, the tests show that the anodized coatings modified with TiO_2 particles have a very high corrosion resistance to the acidic facade cleaner.

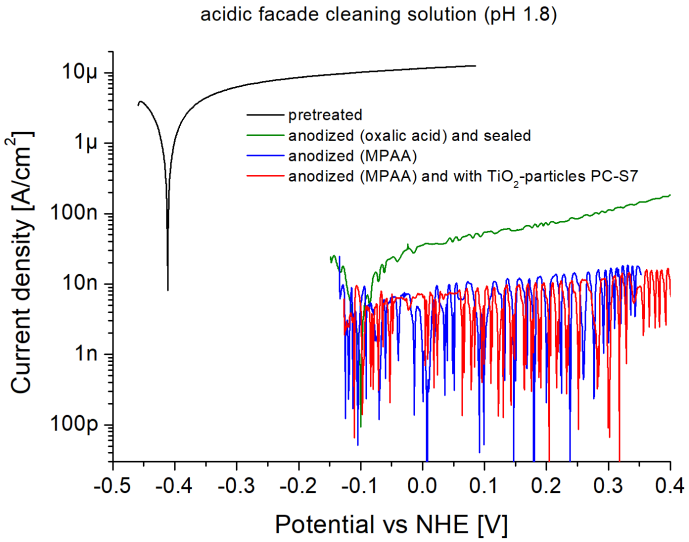

Figure 11. Potentiodynamic polarization curves of AlMg1 samples treated with different processes.

4. Summary and Conclusions

Within the frame of the study, structured, meso- and macroporous anodized layers were generated by a modified phosphoric acid anodizing process. The subsequent incorporation of titania particles was performed by dip coating from water-based systems. Depending on the dip-coating parameters, the porous anodized layers can be filled up to 50 % with functionalized particles. The testing of the photocatalytic properties according to ISO 22197-1 certifies a high photocatalytic activity of these layers with rPCE values of up to 8.4, thus clearly exceeding the minimum requirement of $\geq$2. The corrosion investigations in an acidic aluminum and facade cleaner reveals a significant increase in the corrosion resistance from the anodization plus functionalization. In particular, the measurements show that the incorporation of the TiO_2 particles can achieve a similar barrier effect as a hot compaction step. However, so far, no long-term tests regarding corrosion resistance, as well as photocatalytic activity, have been carried out. Regarding the efficiency of the photocatalytic effect, it should be mentioned that the reduction in NO_x cannot be completely solved by functionalized claddings. Calculations based on typical deposition rates indicate a NO_x degradation rate of a few percent (<10 %) [37]. At first glance, this appears to be low, however, other actions such as the definition of environmental zones are certified to be less effective, with only a 4 % reduction in NO_x values [38]. Hence, a photocatalytically active anodized layer can be a useful component for the reduction in NO_x levels in urban areas.

Author Contributions: Conceptualization, S.B. and S.L.; methodology, S.B. and A.P.; validation, S.B., R.J. and A.P.; formal analysis, S.B.; investigation, R.J. and A.P.; resources, S.B. and A.P.; writing—original draft preparation, S.L.; writing—review and editing, S.B., J.Z.B. and W.F.; visualization, S.B. and S.L.; supervision, S.B., S.L. and W.F.; project administration, S.B. and W.F.; funding acquisition, J.Z.B., S.L. and W.F. All authors have read and agreed to the published version of the manuscript.

Funding: The authors gratefully thank the German Federal Ministry for Economic Affairs and Climate Action (BMWK) for the financial support of the project under grant number 20136 N via the German Federation of Industrial Research Associations (AiF) by a decision of the German Bundestag.

Data Availability Statement: The data presented in this study are available on request from the corresponding author.

Conflicts of Interest: The authors declare no conflict of interest. The funders had no role in the design of the study; in the collection, analyses, or interpretation of data; in the writing of the manuscript; or in the decision to publish the results.

Abbreviations

The following abbreviations are used in this manuscript:

DLS	Dynamic light scattering
DoE	Design of experiments
MPAA	Modified phosphoric acid anodization
rPCE	Relative photocatalytic efficiency
UBA	German Federal Environment Agency
WHO	World Health Organization

References

1. Umweltbundesamt. Available online: https://www.umweltbundesamt.de/en/topics/air/air-pollutants-at-a-glance/nitrogen-dioxide (accessed on 3 November 2022).
2. World Health Oganization. *WHO Global Air Quality Guidelines: Particulate Matter (PM2.5 and PM10), Ozone, Nitrogen Dioxide, Sulfur Dioxide and Carbon*; WHO: Geneva, Switzerland, 2021.
3. Verband der Mineralfarbenindustrie e. V. Available online: Https://www.vdmi.de/en/products/applied-photocatalysis/product-range/photoactive-construction-materials/ (accessed on 3 November 2022).
4. Chen, J.; Poon, C. Photocatalytic construction and building materials: From fundamentals to applications. *Build. Environ.* **2009**, *44*, 1899–1906. https://doi.org/10.1016/j.buildenv.2009.01.002.
5. Zhong, L.; Haghighat, F. Photocatalytic air cleaners and materials technologies—Abilities and limitations. *Build. Environ.* **2015**, *91*, 191–203. https://doi.org/10.1016/j.buildenv.2015.01.033.
6. Hamidi, F.; Aslani, F. TiO_2-based Photocatalytic Cementitious Composites: Materials, Properties, Influential Parameters, and Assessment Techniques. *Nanomaterials* **2019**, *9*, 1444. https://doi.org/10.3390/nano9101444.
7. Kammer, C. *Aluminium Handbook: Vol. 1: Fundamentals and Materials*, 1st ed.; Aluminium-Verlag: Dusseldorf, Germany, 2003.
8. Spooner, R.C. The Anodic Treatment of Aluminum in Sulfuric Acid Solutions. *J. Electrochem. Soc.* **1955**, *102*, 156–162.
9. O'Sullivan, J.P.; Wood, G.C. The morphology and mechanism of formation of porous anodic films on aluminium. *Roc. R. Soc. Lond. A* **1970**, *317*, 511–543. https://doi.org/10.1098/rspa.1970.0129.
10. Ono, S.; Saito, M.; Asoh, H.T. Self-ordering of anodic porous alumina formed in organic acid electrolytes. *Electrochim. Acta* **2005**, *51*, *5*, 827–833.
11. Houser, J.E. Modeling the Steady-State Growth of Porous Anodic Alumina. Ph.D. Thesis, Iowa State University, Ames, IN, USA, 2008.
12. Paz Martínez-Viademonte, M.; Abrahami, S.T.; Hack, T.; Burchardt, M.; Terryn, H. A Review on Anodizing of Aerospace Aluminum Alloys for Corrosion Protection. *Coatings* **2020**, *10*, 1106. https://doi.org/10.3390/coatings10111106.
13. Schneider, M.; Fuerbeth, W. Anodizing—The pore makes the difference. *Mater. Corros.* **2022**, *73*, 1752–1765. https://doi.org/10.1002/maco.202213324.
14. Henley, V.F. *Anodic Oxidation of Aluminium and Its Alloys*, 1st ed.; Pergamon Press: New York, NY, USA, 1982.
15. Belwalkar, A.; Grasing, E.; Van Geertruyden, W.; Huang, Z.; Misiolek, W.Z. Effect of processing parameters on pore structure and thickness of anodic aluminum oxide (AAO) tubular membranes. *J. Membr. Sci.* **2008**, *319*, 192–198.
16. Ono, S.; Masuko, N. Evaluation of pore diameter of anodic porous films formed on aluminum. *Surf. Coat. Technol.* **2003**, *169–170*, 139–142.
17. Ramirez, O.; Queiroz, F.M.; Tunes, M.; Antunes, R.; Rodrigues, C.; Lanzutti, A.; Pogatscher, S.; Olivier, M.-G.; De Melo, H.G. Tartaric-sulphuric acid anodized clad AA2024-T3 post-treated in Ce-containing solutions at different temperatures: Corrosion behaviour and Ce ions distribution. *Appl. Surf. Sci.* **2020**, *534*, 147634. https://doi.org/10.1016/j.apsusc.2020.147634.
18. Pinner, R.; Sheasby, P.G. *The Surface Treatment and Finishing of Aluminium and Its Alloys*, 6th ed.; ASM International: Almere, The Netherlands, 2001.
19. Terada, M.; Queiroz, F.M.; Aguiar, D.B.S.; Ayusso, V.H.; Costenaro, H.; Olivier, M.-G.; De Melo, H.G.; Costa, I. Corrosion resistance of tartaric-sulfuric acid anodized AA2024-T3 sealed with Ce and protected with hybrid sol–gel coating. *Surf. Coat. Technol.* **2019**, *372*, 422–426. https://doi.org/10.101/j.surfcoat.2019.05.028.
20. Fedel, M.; Franch, J.; Rossi, S. Effect of thickness and sealing treatments on the corrosion protection properties of anodic oxide coatings on AA5005. *Surf. Coat. Technol.* **2021**, *408*, 126761. https://doi.org/10.1016/j.surfcoat.2020.126761.
21. Mann, R.; Hansal, S.; Hansal, W.E.G. Nanoparticle incorporation in plasma-electrolytic oxidation. *Int. J. Surf. Eng. Coat.* **2016**, *94*, 131–138.
22. Fori, B.; Taberna, P.-L.; Arurault, L.; Bonino, J.P.; Gazeau, C.; Bares, P. Electrophoretic impregnation of porous anodic aluminum oxide film by silica. *Colloids Surf.* **2012**, *A 415*, 187–194.
23. Schüth, F.; Sing, K.S.W.; Weitkamp, J. *Handbook of Porous Solids*, 3rd ed.; Wiley-VCH: Weinheim, Germany, 2002.
24. US Research Nanomaterials Inc. Available online: https://www.us-nano.com/inc/sdetail/484 (accessed on 3 November 2022).
25. Nyacol Nano Technologies Inc. Available online: https://www.nyacol.com/products/titanium-dioxide/ (accessed on 3 November 2022).

26. Etacheri, V.; Di Valentin, C.; Schneider, J.; Bahnemann, D.; Pillai, S.C. Visible-light Activation of TiO2 Photocatalysts: Advances in Theory and Experiments, *J. Photochem. Photobiol. C* **2015**, *25*, 1–29. https://doi.org/10.1016/j.jphotochemrev.2015.08.003.
27. Schneider, J.; Matsuoka, M.; Takeuchi, M.; Zhang, J.; Horiuchi, Y.; Anpo, M.; Bahnemann, D.W. Understanding TiO_2 Photocatalysis: Mechanisms and Materials. *Chem. Rev.* **2014**, *114*, 9919–9986. https://doi.org./10.1021/cr5001892.
28. Schneider, M.; Kremmer, K.; Weidmann, S.K.; Fuerbeth, W. Interplay between parameter variation and oxide structure of a modified PAA process. *Surf. Interface Anal.* **2013**, *45*, 1503–1509. https://doi.org/10.1002/sia.5248.
29. Schneider, M; Kremmer, K.; Weidmann, S.K.; Fuerbeth, W. Particle reinforced open porous anodizing layers on AA5005. *Mater. Corr.* **2017**, *68*, 1090–1098. https://doi.org/10.1002/maco.201609389.
30. Landau, L.D.; Levich, B.G. Dragging of a liquid by a moving plate. *Acta Physiochim. U.R.S.S.* **1942**, *8*, 42–54.
31. German Federation for Applied Photocatalysis. *V*oluntary commitment of the manufacturers of photocatalytically active products to achieve a minimum activity for the NO degradation on photocatalytically active surfaces. Available online: https://www.vdmi.de/en/products/applied-photocatalysis/voluntary-commitment/voluntary-commitment/?= (accessed on 4 November 2022).
32. Masuda, H.; Hasegwa, F.; Ono, S. Self-Ordering of Cell Arrangement of Anodic Porous Alumina Formed in Sulfuric Acid Solution. *J. Electrochem. Soc.* **1997**, *144*, 127–130. https://doi.org/10.1149/1.1837634.
33. Vorobyova, A.I.; Outkina, E.A. Study of pillar microstructure formation with anodic oxides. *Thin Solid Film.* **1998**, *324*, 1–10. https://doi.org/10.1016/S0040-6090(97)01194-2.
34. Ye, J.; Yin, Q.; Zhou, Y. Superhydrophilicity of anodic aluminum oxide films: From "honeycomb" to "bird's nest". *Thin Solid Film.* **2009**, *517*, 6012–6015.
35. Kim, Y.-C.; Quint, B.; Kessler, R.W.; Oelkrug, D. Structural properties of electrochemically designed porous oxide films on AlMg1. *J. Electroanal. Chem.* **1999**, *468*, 121–126.
36. Xu, Y.-f.; Liu, H.; Li, X.-j.; Kang, W.-m., Cheng, B.-w.; Li, X.-j. A novel method for fabricating self-ordered porous anodic alumina with wide interpore distance using phosphoric/oxalic acid mixed electrolyte. *Mater. Lett.* **2015**, *151*, 79–81. https://doi.org/10.1016/j.matlet.2015.03.049.
37. Gallus, M.; Ciuraru, R.; Mothes, F.; Akylas, V.; Barmpas, F.; Beeldens, A.; Bernard, F.; Boonen, E.; Boréave, A.; Cazaunau, M.; et al. Photocatalytic abatement results from a model street canyon. *Environ. Sci. Pollut. Res.* **2015**, *22*, 18185–18196. https://doi.org/10.1007/s11356-015-4926-4.
38. Morfeld, P.; Groneberg, D.A.; Spallek, M.F. Effectiveness of low emission zones: Large scale analysis of changes in environmental NO_2, NO and NO_x concentrations in 17 German cities. *PLoS ONE* **2014**, *9*, e102999. https://doi.org/10.1371/journal.pone.0102999.